ZOOLOGICAL RESEARCH

Tube-nosed variations–a new species of the genus *Murina* (Chiroptera: Vespertilionidae) from China

DEAR EDITOR,

During a survey in 2014, several tube-nosed bats (Vespertilionidae: Murininae: *Murina*) were collected in Sichuan Province. Based on morphological characters, these bats did not match any species previously recorded from China. Morphometric analyses and phylogenetic inference based on mitochondrial and nuclear gene sequences indicated that they represented a new species, named here as *Murina jinchui* **sp. nov**. Although the new species is presently known only from Wolong National Nature Reserve, it is unlikely to be a rare species in the area based on our capture frequencies.

Characterized by tubular nostrils and relatively well-developed anterior upper premolars, the Old World subfamily of vespertilionid bats, Murininae Miller, 1907, is rich in cryptic species. Typically, these species are rare in collections, which have contributed to our poor understanding of their diversity and distribution. Simmons (2005) listed 17 species within the subfamily, but several new species have been described since due to an increase in survey efforts, improved capture methods, re-evaluation of taxonomically informative characters, and species delimitations using DNA barcoding (Csorba et al., 2011; Eger & Lim, 2011; Francis et al., 2010). As such, 39 species are currently recognized based on taxonomic revisions and new species descriptions (Chen et al., 2017; Csorba et al., 2007, 2011 Eger & Lim, 2011; Francis & Eger, 2012; Furey et al., 2009; He et al., 2015; Kruskop & Eger, 2008; Kuo et al., 2009; Maeda & Matsumura, 1998; Ruedi et al., 2012; Soisook et al., 2013a, 2013b Son et al., 2015; Zeng et al., 2018). In the last decade, intensive survey efforts and morphological and molecular studies have resulted in the description of nine new *Murina* species from China alone, namely *M. bicolor*, *M. gracilis*, and *M. recondita* from Taiwan (Kuo et al., 2009), *M. chrysochaetes*, *M. lorelieae*, and *M. shuipuensis* from Guangxi and Guizhou (Eger & Lim, 2011), and *M. fanjingshanensis* (He et al., 2015), *M. rongjiangensis* (Chen et al., 2017), and *M. liboensis* (Zeng et al., 2018) from Guizhou. Thus, at least 19 species belonging to the genus *Murina* are currently known from China (Chen et al., 2017; Eger & Lim, 2011; He et al., 2015; Jiang et al., 2015; Kuo et al., 2009; Liu & Wu, 2019; Zeng et al., 2018).

In 2014, several small-sized and impressively colored *Murina* individuals were collected during field surveys in Sichuan Province (all field surveys and sample collection protocols complied with the current laws of Sichuan Province). Morphological and molecular biological examinations revealed them to be distinct from all other recognized *Murina* taxa; therefore, they are described herein as a new species.

For morphometric analysis, we examined 224 specimens of *Murina* deposited in 12 collections (see list of specimens in Supplementary Material (Appendix I)). Six external measurements (to the nearest 0.1 mm), body mass (to the nearest 0.1 g), and 16 craniodental measurements (to the nearest 0.01 mm) were recorded by the same author. Definitions and details of measurements are listed in the Table 1 and Supplementary Material (Methods).

We performed principal component analysis (PCA) and discriminant analysis of principal components (DAPC) (Jombart, 2008; Jombart et al., 2010) for species discrimination based on external and craniodental measurements. For both PCA and DAPC, the sexes were analysed separately because sexual dimorphism is noted in

Received: 04 August 2019; Accepted: 15 November 2019; Online: 11 December 2019

Foundation items: This study was financially supported by the National Natural Science Foundation of China (NSFC, 31672258, 31670381, 31970394), NSFC Major International (Regional) Joint Research Project Grant (31110103910), and Guangzhou University's 2017 Training Program for Young High-Achieving Personnel (BJ201707). The research of Gabor Csorba received support from the Hungarian Scientific Research Fund–OTKA K112440, National Research, Development and Innovation Fund of Hungary NKFIH KH130360 and from the SYNTHESYS Project, which is financed by the European Community Research Infrastructure Action under the FP7 "Capacities" Program

DOI: 10.24272/j.issn.2095-8137.2020.009

Table 1 Selected external and craniodental measurements (mm) of *Murina jinchui* sp. nov and four closely related *Murina* species

Item	*Murina jinchui* **sp. nov.**			*M. rongjiangensis*		*M. shuipuensis*		*M. fanjing-shanensis*	*M. leucogaster*	
	♀♀	♂♂	*t*-value	♀♀	♂♂	♀♀	♂♂	♂	♀♀	♂
GTL	16.47 (3) (16.10–16.86)	15.73 (3) (15.66–15.83)	3.25*	16.27±0.3 (5) (15.88–16.71)	15.76±0.29 (5) (15.32–16.04)	16.00, 16.05 (2)	15.82 (3) (15.60–16.15)	19.22 (1)	19.14 (3) (18.77–19.33)	19.5 (1)
CCL	14.42 (3) (14.34–14.48)	13.65 (3) (13.58–13.68)	14.5*	14.38±0.45 (5) (13.73–14.98)	13.84±0.21 (5) (13.49–14.03)	13.92, 14.26 (2)	13.90 (3) (13.82–14.00)	16.13 (1)	16.81 (3) (16.52–17.13)	16.84 (1)
CBL	15.81 (3) (15.50–16.07)	15.14 (3) (15.12–15.15)		15.19±0.48 (5) (14.51–15.78)	14.74±0.14 (5) (14.60–14.95)	14.65, 15.06 (2)	14.64 (3) (14.53–14.83)	17.62 (1)	17.85 (3) (17.60–18.09)	17.91 (1)
BCW	7.64 (3) (7.60–7.72)	7.18 (3) (7.15–7.22)	10.18*	7.63 ±0.21 (5) (7.45–7.94)	7.57±0.1 (5) (7.44–7.71)	7.31, 7.47 (2)	7.33 (3) (7.14–7.42)	9.43 (1)	8.77 (3) (8.17–9.10)	8.77 (1)
BCH	7.54 (3) (7.43–7.69)	7.26 (3) (7.04–7.41)	2.05NS	7.4 ±0.25 (5) (7.00–7.64)	7.2±0.15 (5) (7.00–7.37)	6.98, 7.13 (2)	6.96 (3) (6.78–7.22)	8.74 (1)	8.27 (3) (8.13–8.34)	8.16 (1)
ZYW	8.64 (3) (8.53–8.79)	8.55 (3) (8.49–8.60)	0.88NS	9.08 ±0.26 (5) (8.66–9.37)	8.67±0.26 (5) (8.47–9.06)	8.58, 8.70 (2)	8.32 (3) (8.06–8.60)	9.22 (1)	10.74 (3) (10.48–10.99)	10.84 (1)
MAW	8.01 (3) (7.94–8.10)	7.64 (3) (7.54–7.83)	3.53*	7.97 ±0.2 (5) (7.69–8.19)	7.74±0.16 (5) (7.60–7.99)	7.56, 7.68 (2)	7.47 (3) (7.37–7.61)	8.66 (1)	9.10 (3) (8.85–9.21)	9.31 (1)
PL	7.31 (3) (7.09–7.58)	7.15 (3) (7.03–7.33)	0.92NS	7.00 ±0.16 (5) (6.79–7.19)	6.8±0.16 (5) (6.70–7.08)	7.50, 7.56 (2)	7.47 (3) (7.13–7.69)	9.22 (1)	8.66 (3) (8.44–8.97)	8.74 (1)
IOW	4.41 (3) (4.32–4.52)	4.24 (3) (4.05–4.50)	1.15NS	4.69 ±0.13 (5) (4.54–4.90)	4.54±0.15 (5) (4.30–4.70)	4.33, 4.57 (2)	4.47 (3) (4.30–4.65)	5.46 (1)	5.39 (3) (5.10–5.69)	5.50 (1)
CM^3L	5.52 (3) (5.47–5.58)	5.21 (3) (5.12–5.32)	4.68*	5.31 ±0.14 (5) (5.13–5.47)	5.06±0.06 (5) (4.97–5.13)	5.28, 5.33 (2)	5.33 (3) (5.25–5.39)	6.35 (1)	6.46 (3) (6.36–6.53)	6.34 (1)
CCW	4.05 (3) (3.99–4.16)	3.79 (3) (3.65–3.88)	2.89*	4.26 ±0.15 (5) (4.02–4.38)	3.92±0.14 (5) (3.80–4.13)	3.94, 4.08 (2)	3.92 (3) (3.90–3.94)	4.70 (1)	4.74 (3) (4.62–4.91)	4.91 (1)
M^3M^3W	5.92 (3) (5.88–5.95)	5.44 (3) (5.32–5.51)	7.28*	5.71 ±0.18 (5) (5.49–5.95)	5.53±0.19 (5) (5.27–5.76)	5.40, 5.57 (2)	5.49 (3) (5.38–5.54)	6.54 (1)	6.51 (3) (6.04–6.79)	6.66 (1)
RCM	0.68 (3) (0.67–0.71)	0.70 (3) (0.69–0.70)	–0.97NS	0.75 ±0.02 (5) (0.73–0.78)	0.71±0.02 (5) (0.69–0.73)	0.73, 0.73 (2)	0.71 (3) (0.70–0.73)	0.72 (1)	0.73 (3) (0.69–0.81)	0.74 (1)
LCM_3L	5.78 (3) (5.68–5.85)	5.68 (3) (5.57–5.75)	1.32NS	5.59 ±0.11 (5) (5.44–5.71)	5.52±0.11 (5) (5.42–5.68)	5.57, 5.61 (2)	5.65 (3) (5.53–5.75)	–	6.73 (3) (6.49–6.85)	6.58 (1)
ML	11.41 (3) (11.34–11.49)	10.79 (3) (10.68–10.90)	8.08*	11.25 ±0.32 (5) (10.98–11.78)	10.65±0.23 (5) (10.38–11.00)	10.84, 10.98 (2)	10.75 (3) (10.63–10.83)	–	12.99 (3) (12.71–13.22)	12.98 (1)
CPH	3.95 (3) (3.90–4.01)	3.37 (3) (3.34–3.42)	14.21*	3.8 ±0.19 (5) (3.49–3.99)	3.48±0.23 (5) (3.24–3.80)	3.73, 3.88 (2)	3.51 (3) (3.39–3.68)	–	4.86 (3) (4.62–5.02)	4.97 (1)
Wt	7.3 (3) (7.1–7.5)	4.9 (3) (4.5–5.2)		6.8±1.09 (5) (5.0–7.8)	5.0±0.26 (5) (4.7–5.4)	4.3, 5.1 (2)	4.7 (3) (4.3–5.0)	9.0 (1)	–	10.9 (1)
HB	44.7 (3) (43.0–45.7)	40.1 (3) (39.7–40.4)	5.45*	43.5 ± 2.48 (5) (40.6–46.7)	38.8 ± 4.86 (5) (34.0–46.5)	40.6, 40.9 (2)	41.4 (3) (40.0–43.3)	46.3 (1)	47.7 (3) (44.4–51.4)	50.3 (1)
T	34.9 (3) (33.0–38.4)	34.9 (3) (33.6–36.0)	0.01NS	34.9 ± 1.90 (5) (32.9–37.3)	33.8 ± 1.38 (5) (32.3–35.4)	32.0, 38.4 (2)	33.5 (3) (31.9–36.6)	39.7 (1)	40.1 (3) (37.7–41.5)	39.3 (1)
E	15.3 (3) (14.4–16.1)	14.7 (3) (14.4–15.1)	1.08NS	11.2 ± 0.72 (5) (10.2–11.9)	10.6 ± 0.98 (5) (9.0–11.6)	11.7, 13.4 (2)	11.6 (3) (10.7–12.4)	15.3 (1)	12.8 (3) (12.4–13.3)	13.8 (1)
HF	8.2 (3) (7.2–9.4)	7.5 (3) (7.4–7.7)	1.03NS	7.8 1.07 (5) (5.9–8.7)	7.5 ± 0.89 (5) (6.1–8.4)	8.7, 9.1 (2)	8.5 (3) (7.8–9.1)	8.5 (1)	9.6 (3) (8.9–10.3)	11.4 (1)
FA	36.3 (3) (36.1–36.4)	33.5 (3) (32.4–34.6)	4.26*	33.0 ±1.36 (5) (30.6–34.0)	31.6 ± 0.81 (5) (31.0–32.7)	30.0, 32.7 (2)	30.8 (3) (29.7–31.9)	42.6 (1)	43.6 (3) (43.0–44.2)	41.5 (1)

Continued

Item	*Murina jinchui* **sp. nov.**			*M. rongjiangensis*		*M. shuipuensis*		*M. fanjing-shanensis*	*M. leucogaster*	
	♀♀	♂♂	*t*-value	♀♀	♂♂	♀♀	♂♂	♂	♀♀	♂
Tib	16.4 (3) (16.4–16.5)	15.3 (3) (14.7–16.0)	3.01*	14.8 ± 0.72 (5) (13.9–15.6)	15.0 ± 0.63 (5) (14.2–15.7)	14.5, 15.2 (2)	14.7 (3) (13.8–16.2)	19.5 (1)	19.3 (3) (18.3–19.9)	17.9 (1)

Values are given as Means±*SD* (if *n*>5), and minimum-maximum (min -max). *t*-value is from Students *t*-test between sexes when distribution of measurement fits normality, and * and NS represent *P*<0.05 and non-significant result, respectively. Abbreviations and definitions for measurements are as followed: HB: Total length–from the tip of the face/chin to the anus; T: Tail vertebrae length–from the tip of the tail to the beginning of the tail vertebrae; E: Ear length–from the notch at the base of the ear conch to the tip of the pinna; HF: Hind foot length–from the heel to the tip of the longest toe, including the claw; Tib: Length of tibia–from the knee to the ankle; FA: Forearm length–from the elbow to the wrist with both joints folded; GTL: Greatest length of skull–from the posterior edge of the skull to the front of the incisors; CCL: Condylocanine length–from the exoccipital condyle to the most anterior part of the canine; CBL: Condylobasal length–from the exoccipital condyle to the posterior rim of alveolus of the first upper incisor; BCW: Braincase width–greatest width across the braincase; BCH: Braincase height–from the basisphenoid at the level of the hamular processes to the highest part of the skull, including the sagittal crest (if present); ZYW: Zygomatic width–the greatest width of the skull across the zygomatic arches; MAW: Mastoid width–the greatest distance across the mastoid region; PL: Palatal length–from the anterior palatal emargination to the midpoint of the posterior palatal emargination; IOW: Interorbital width–least width of the interorbital constriction; CM^3L: Length of maxillary toothrow–from the front of the canine to the posterior edge of the 3rd upper molar; CCW: Greatest breadth across the upper canines; M^3M^3W: Width across upper molars–greatest width measured across the outer edges of the second upper molars; RCM: Ratio of CCW to M^3M^3W; LCM_3L: Length of mandibular toothrow–from the front of the canine to the posterior edge of the 3rd lower molar; ML: Greatest length of mandible–greatest length measured from the posterior edge of the mandibular condyles to the front of the lower incisors; CPH: Coronoid process height–measured from the inferior surface of the angular process of the ramus to the tip of the coronoid process.

several *Murina* species (Kuo et al., 2009; Son et al., 2015), including the new one (Table 1; Supplementary Figure S1 and Table S1). We also replicated our multivariate statistical analyses in the monophyletic clade formed by *M. leucogaster*, *M. shuipuensis*, *M. rongjiangensis*, and the new species. In addition, due to their similarities in size and skull proportions, *M. shuipuensis*, *M. rongjiangensis*, and the new species were also compared using analysis of variance (ANOVA). All analyses were performed using the "phych" and "adegenet" packages in R (Jombart, 2008; R Development Core Team, Vienna, www.R-project.org).

For phylogenetic analysis, the partial cytochrome oxidase subunit I (*COI*, 670 bp) and partial nuclear recombination activating protein 2 genes (*Rag2*, 1 339 bp) were selected as molecular markers (Heaney et al., 2012; Kuo et al., 2017; Lack & Bussche, 2010; Roehrs et al., 2010). The *COI* gene was amplified from specimens of all species in this study, whereas the *Rag2* gene was sequenced from single individuals of each species confirmed by our phylogenetic and morphological species determination (GenBank accession Nos.: MN549027–MN549101). All available *COI* and *Rag2* sequences of *Murina* collected from NCBI-nt and our specimens were aligned using MUSCLE (Edgar, 2004). Final alignment was partitioned by different codon positions and the parameters of the best nucleotide substitution models were determined by PartitionFinder2 (Lanfear et al., 2017) using the greedy algorithm (Lanfear et al., 2012). Maximum-likelihood (ML) trees were searched in RAxML v7.4.2 (Stamatakis et al., 2008), and the reliability of nodes was evaluated by 500 rapid bootstrap matrixes.

To describe pelage color, digital photographs of freshly euthanized bats were taken in the field (see details in Supplementary Material). Following Davis & Castleberry (2010), images were color calibrated, and pelage color was described following the Pantone color code with the red-green-blue (RGB) system.

Detailed measurements of all specimens used in this study are listed in Table 1. The PCA based on six external measurements revealed that 76% of total variance could be explained by the first two components (54% and 22% for principal components 1 (PC1) and principal components 2 (PC2), respectively) (Figure 1A). For PC1, all measurements, except for ear length, had high positive loadings, thus reflecting an external overall size effect. PC2 was mostly related to ear size (larger value indicates larger measurement) (Figure 1A, with values provided in Table 2). Although the interspecific patterns revealed by PCA were ambiguous, implying difficulty in species identification based on external measurements only, the PCA results consistently indicated larger females and smaller males within *Murina* species. For PCA of the 16 craniodental measurements, 81% of total variance could be explained by the first two components (57% and 24% for PC1 and PC2, respectively) (Figure 1B). For PC1, 11 measurements had positive loadings (Figure 1B, with values provided in Table 1), suggesting that this PC was mainly related to skull size (smaller bats characterized by lower PC1 scores). Thus, with the exception of *M. leucogaster*, most *Murina* species with *suilla*-type dentition (crown area of upper canine less than that of P^4) had smaller skulls than those species with *cyclotis*-type dental characters (crown area of upper canine equal to or larger than that of P^4) (Figure 1B). For PC2, most measurements had low loadings, except for braincase width (BCW), mastoid width (MAW), and interorbital width (IOW) (Figure 1B and Table 1). Unlike the ambiguous pattern found for external measurements, PCA based on craniodental measurements revealed a more

noticeable interspecific relationship, with six skull-size assemblages identified: i.e., (1) *M. leucogaster*; (2) *M. aurata*; (3) all taxa with *cyclotis*-type dentition included in this study; (4) *M. eleryi*+*M. chrysochaetes*; (5) *M. shuipuensis*+*M. rongjiangensis*+new species; and (6) "*M. jaintiana*+*M. beelzebub*+*M. feae*" (Figure 1B).

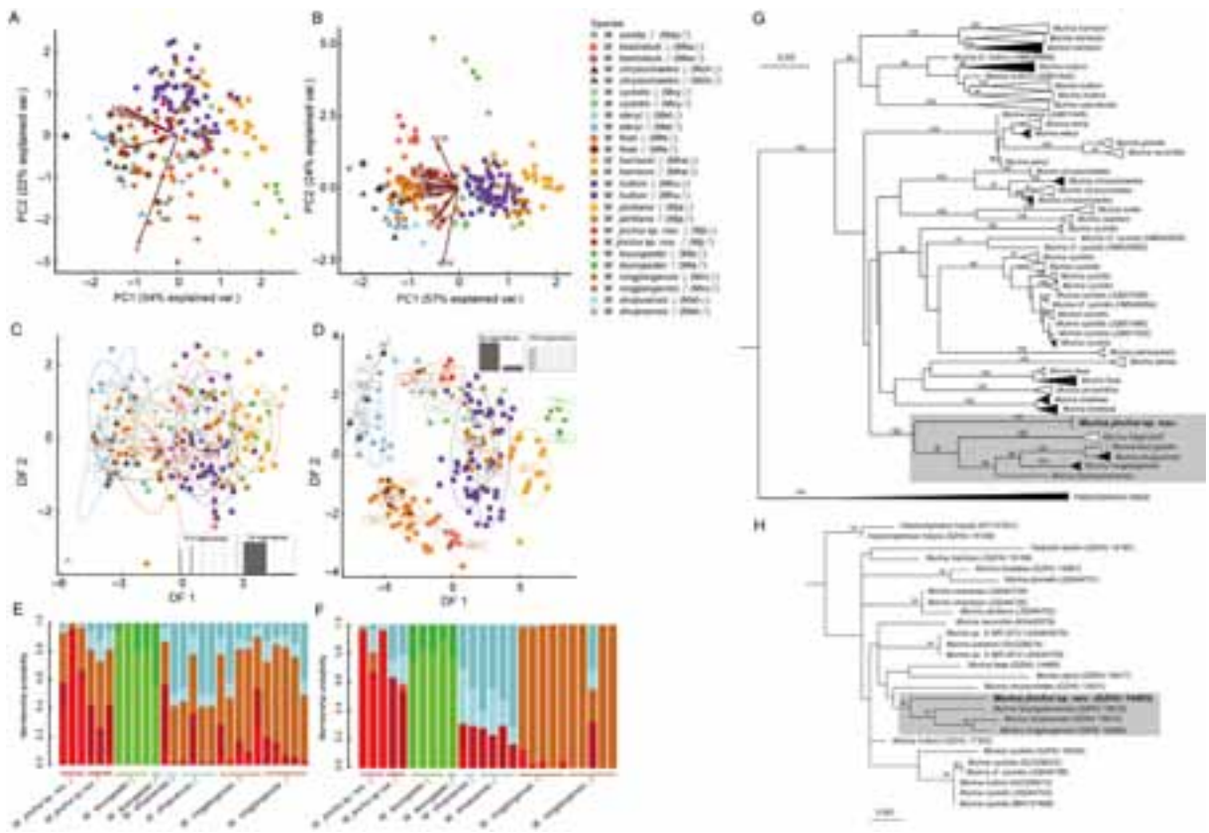

Figure 1 Two-dimensional PCA and DAPC plots and maximum-likelihood phylogenetic trees

A, B: PCA plots for *M. aurata*, *M. chrysochaetes*, *M. cyclotis*, *M. eleryi*, *M. harrisoni*, *M. huttoni*, *Murina jinchui* **sp**. **nov**., *M. leucogaster*, *M. rongjiangensis*, *M. shuipuensis*, *M. jaintiana*, *M. beelzebub*, and *M. feae* showing projections of individual specimens and variable loadings on first two principal components. C, D: Projections of 224 specimens and variable loadings on two DFs obtained from external and craniodental measurements. E, F: Posterior probabilities of the same 26 specimens reclassified following analysis of phylogenetic clade of *M. leucogaster*, *Murina jinchui* **sp. nov.**, M. *shuipuensis*, and *M. rongjiangensis* using DAPC. According to species and sex, eight groups were predetermined in this DAPC. Maximum-likelihood trees based on mitochondrial *COI* (G) and nuclear *Rag2* (H) sequences for the subfamily Murininae. Triangles in (G) represent clusters of multiple specimens, with horizontal dimension proportional to amount of sequence divergence. Solid triangles indicate newly generated *COI* sequences. Numbers above branches indicate level of bootstrap support >50% for the branch.

We used the PC1 and PC2 values from the external and craniodental analyses for DAPC, with the results together explaining 87% and 90% of total variance, respectively. Among the original external variables, HB, T, and FA had high positive loadings on discriminant function 1 (DF1), whereas HB and T had high positive loadings on discriminant function 2 (DF2) (Table 2). For craniodental DAPC analysis, greatest length of skull (GTL), condylocanine length (CCL), and greatest length of mandible (ML) contributed substantially to DF1, whereas braincase height (BCH) and mastoid width (MAW) contributed substantially to DF2 (Table 2). Similar to the PCA plots of external variables, the DAPC plots revealed an ambiguous pattern, with most taxa overlapping (Figure 1C). Nevertheless, based on an increase in discriminant power, the pattern of the craniodental DAPC plots was more distinguishable than that of the PCA plots, although most were still partially overlaid (Figure 1D). Similar to the PCA pattern from craniodental measurements, a noticeable interspecific relationship emerged, with five skull-size assemblages identified, including: (1) *M. leucogaster*; (2) all *cyclotis*-type taxa included in this study; (3) *M. aurata*+*M. eleryi*+*M. chrysochaetes*; (4) *M. shuipuensis*+*M. rongjiangensis*+new species; and (5) "*M. jaintiana*+*M. beelzebub*+*M. feae*" (Figure 1D). Based on DAPC reclassification of inference of clades, including *M. shuipuensis*, *M. rongjiangensis*, *M. leucogaster*, and the new species, craniodental DAPC revealed higher

Table 2 Variable loadings on principal components (PCs) and contribution of original variables in discriminant functions (DFs) from external and craniodental measurements, respectively

	PCA				DAPC			
	PC 1	PC 2	PC 1	PC 2	DF 1	DF 2	DF 1	DF 2
HB	**0.843**	0.222	–	–	**0.307**	**0.451**	–	–
T	**0.696**	0.433	–	–	**0.385**	**0.531**	–	–
E	0.255	**0.953**	–	–	0.027	0.004	–	–
HF	**0.749**	0.201	–	–	0.011	0.002	–	–
FA	**0.877**	0.220	–	–	**0.211**	0.007	–	–
Tib	**0.795**	0.242	–	–	0.060	0.003	–	–
GTL	–	–	**0.823**	0.482	–	–	**0.231**	0.001
CCL	–	–	**0.870**	0.447	–	–	**0.210**	0.004
BCW	–	–	0.529	**0.716**	–	–	0.018	0.001
BCH	–	–	0.534	0.386	–	–	0.065	**0.582**
ZYW	–	–	**0.828**	0.459	–	–	0.093	0.013
MAW	–	–	**0.364**	0.549	–	–	0.008	**0.365**
IOW	–	–	–	**0.925**	–	–	0.002	0.001
CM^3L	–	–	**0.868**	0.362	–	–	0.037	0.002
CCW	–	–	**0.922**	0.310	–	–	0.031	0.003
M^3M^3W	–	–	0.741	0.16	–	–	0.029	0.010
RCM	–	–	**0.834**	–0.103	–	–	0.001	0.001
LC_1M_3L	–	–	**0.859**	0.295	–	–	0.044	0.015
ML	–	–	**0.866**	0.428	–	–	**0.177**	0.001
CPH	–	–	**0.880**	0.358	–	–	0.055	0.004

For abbreviations, see text and Table 1. Bold text indicates high loading of variable on related PC and DF. –: Not available.

power in determining species and sex than the external one, nevertheless both received an ambiguous reclassification in determining *M. shuipuensis*, *M. rongjiangensis*, and our new species and their sex (PP<0.80 for the most likely group and its actual allocation) (Figure 1E–F). These results indicate external and craniodental similarity as well as difficulty in identification using morphological or craniodental measurements alone.

COI alignment spanned 671 bp, including 265 and 256 variable sites and parsimony informative sites, respectively. *Rag2* alignment covered 1 339 bp, including 127 variable sites and 58 parsimony informative sites. For both alignments, the best partitioning scheme selected was one separating each codon position into a partition. For ML analyses, the best nucleotide substitution models for the first, second, and third partitions of *COI* were TIM+G, HKY, and GTR+G, respectively, whereas the best nucleotide substitution models for three position of *Rag2* were TRN+I, HKY, and TIM+G, respectively. The ML trees recovered the genus *Murina* as a well-supported (BS=100) monophyletic group (Figure 1G–H). The phylogenetic reconstructions of the *COI* sequences revealed similar species groups as reported by Francis & Eger (2012) and Eger & Lim (2011). Within the genus, a robust clade, including several *Murina* species known from southern China, emerged (highlighted with gray rectangle in Figure 1G, BS=100). The new species formed a basal, well-supported, monophyletic group within this clade, which included *M. rongjiangensis*, *M. fanjingshanensis*, *M. shuipuensis, M. hilgendorfi*, and *M. leucogaster*. Due to the limited number of phylogenetically informative variations, phylogeny using *Rag2* resulted in a more ambiguous topology (Figure 1H). However, a well-supported clade (highlighted with gray rectangle in Figure 1H, BS=82), similar to the species assemblage based on the *COI* marker, also emerged, with the basal position of the new species supported (Figure 1GH). Hence, the distinctiveness of the new species was supported by both mitochondrial and nuclear markers.

Taxonomic account

Murina jinchui **sp. nov.** Yu, Csorba, Wu (Figures 1–2; Table 1; Supplementary Table S1)

Common names: Jinchu's Tube-nosed Bat (锦矗管鼻蝠, Jinchu Guanbifu).

Holotype: GZHU 14463, adult male, skin and body in alcohol with skull extracted and cleaned, collected on 13 August 2014 by Yi Wu, Feng Li, Bo-Cheng Chen, and Qiu-Ping Zhang. Deposited in the Key Laboratory of Conservation and Application in Biodiversity of South China, School of Life Sciences, Guangzhou University. The nucleotide sequences of the mitochondrial gene *COI* (GenBank accession No. MN549070) and nuclear gene *Rag2* (GenBank accession No. MN549091) were deposited in GenBank.

Paratypes: All paratypes were collected on 13 August 2014 from the type locality. They were preserved in alcohol with their skulls removed, and deposited in the Key Laboratory of Conservation and Application in Biodiversity of South China, School of Life Sciences, Guangzhou University (GZHU 14453 ♀; GZHU 14454 ♀; GZHU 14455 ♀; GZHU 14462 ♂) and the Hungarian Natural History Museum (GZHU 14461=HNHM 2019.1.1. ♂)

Measurements (in mm) and body mass (in g) of holotype: HB, 40.1; T, 36.0; HF, 7.4; E, 14.4; Tib, 14.7; FA, 32.6; GTL, 15.71; CCL, 13.68; CBL, 15.12; BBW, 7.18; BCH, 7.04; ZYW, 8.49; MAW, 7.55; PL, 7.03; IOW, 4.05; CM^3L, 5.32; CCW, 3.88; M^3M^3W, 5.51; LCM_3L, 5.72; GLM, 10.90; CPH, 3.34; Wt, 4.5.

Type locality: Hetaoping Giant Panda Training Base, Wolong National Nature Reserve, Wenchuan County, Sichuan Province, China (N31°4′23″, E103°13′02″), 1 800 m a.s.l..

Diagnosis: Small species of *Murina* (FA: 32.4–36.4 mm; TIB: 15.7–16.9 mm, Table 1, Figure 1; Supplementary Figure S1 and Table S1). Ears rounded and small without notch on posterior edge (Figure 2B). Plagiopatagium attached near base of toe (Figure 2C). Overall color of dorsum brownish gray with banded appearance (Figure 2D); ventral fur goose gray with two bands (Figure 2E). Skull delicate and braincase not globose (Figure 2F). Both upper incisors visible in lateral view; second upper premolar well-developed compared with corresponding canine and anterior premolar (Figure 2F); mesostyles on first and second upper molars moderately developed, with distinct cusp (Figure 2G).

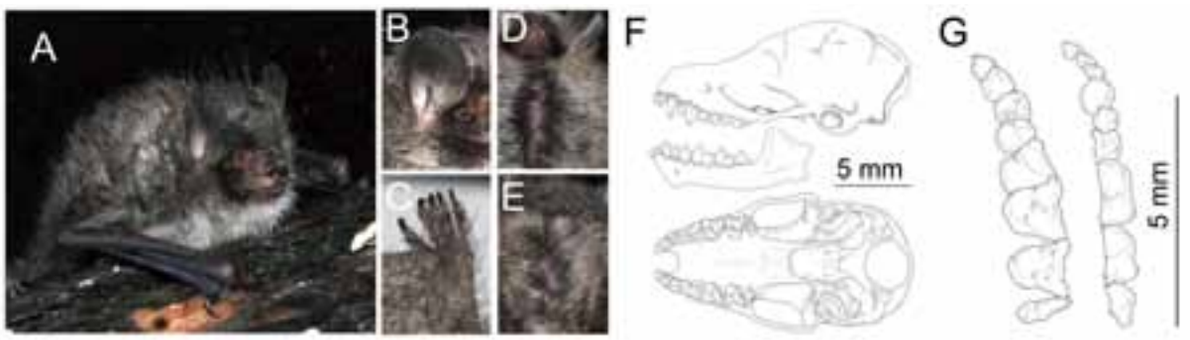

Figure 2 External, skull, and dentition characteristics of *Murina jinchui* sp. nov (holotype, GZHU 14463)

Live individual (A), ear (B), hindfoot (C), dorsal (D) and ventral (E) views of pelage; lateral views of skull and mandible (F); occlusal views of left upper (left) and right lower (right) dentition (G). Scale bars: 5 mm. Photos by Yi Wu (A) and Wen-Hua Yu (B–E).

Description: Small species of *Murina* with '*suilla*-type' dentition. Skin of muzzle, including nose, dark (Figure 2A). Pinnae relatively rounded and large without emargination (Figure 2B). On dorsal surface, basal section of individual hairs black (3 mm, Pantone Process Black C), mid-section brownish gray (1–1.5 mm, Pantone Warm Gray 11C), terminating with dark brown tip (1 mm, Pantone 411C) (Figure 2D). Overall color of dorsum brownish gray (Pantone 410C) (Figure 2A). Underfur overlaid by unicolored warm gray guard hairs (7–8 mm) (3–4 mm, Pantone Warm Gray 11C) (Figure 2D). Upper surface of hind limbs and uropatagium densely furred, particularly along tail and femur, uniformly dark brown. On ventral surface, basal body hairs black (3 mm, Pantone Hexachrome Black C), terminal half progressing to cool gray (Pantone Cool Gray 9 C) (Figure 2E). Ventral guard hairs unicolored gold (7–8 mm, Pantone P7531C) (Figure 2E). Ventral surface of uropatagium covered by short white hairs, rows of papillae with short stiff hairs of similar color as ventral underfur originating from each white dot. Plagiopatagium attached to base of toe. Forearm and metacarpals not furred, short golden hairs present on dorsal surface of thumbs.

Skull small and delicate (Figure 2F; Table 1; Supplementary Table S1), with rostrum sloping gently to forehead (Figure 2F). Laterally, mid-portion of braincase exceeds frontal region in height, braincase not especially domed. No sagittal crest, lambdoid crests relatively weak (Figure 2F). Rostrum deep and pronounced. Depth of nasal emargination exceeds its width, approximately extending to middle of upper canine, outline of emargination varying from smoothly concave to squarish in dorsal view. Basisphenoid pits well-defined, teardrop shaped, elongated, and deep. Zygoma weak, lacking dorsal processes (Figure 2F). Postpalatal emargination with medial projection. Dental formula I 2/3 C 1/1 P 2/2 M 3/3 (Figure 2G). Maxillary toothrows convergent anteriorly (RCM: $\bar{X}$=0.69, range=0.67–0.71, *SD*=0.02, *n*=6). I^2 bicuspid, situated anterior to I^3; I^3 with small secondary cusp lingual to primary cusp (Figure 2F). I^2 and I^3 equal in height, first about half of basal area of second upper incisor; second upper incisor in contact with upper canine, approximately half height of C. Basal area of canine equal to that of first premolar, appearing circular in cross-section. P^2 delicate and pointed, about half P^4 in height; P^4 distinctly higher than C, with basal area twice as large. Metacones of M^1 and M^2 exceeding respective paracones in height. Mesostyle of M^1 and M^2 moderately developed but retaining distinct cusp (Figure 2G). Posterior upper molar lacking metacone, with reduced but distinct postparacrista. Mandible delicate, and lower incisors tricuspid. Lower canine exceeding posterior two premolars in height and basal area, well-developed inner cingulum with anterior-most portion in contact with posterior face of I_3. Basal area of P_2 approximately two-thirds that of P_4, height of P_2 approximately equal to that of P_4. First and second lower molars nyctalodont, with well-developed entoconids. Talonids of M_1 and M_2 equal to respective trigonids in crown area, M_3 talonid half of trigonid (Figure 2F, G).

Comparisons with other taxa: *Murina jinchui* **sp. nov.** possesses *suilla*- type dentition having an upper canine smaller basally than the corresponding posterior premolar, and thus is readily distinguished from all species with *cyclotis*-type dental characters. Among all recognized species with *suilla*-type dentition of the phylogenetically most closely related species, *M. hilgendorfi*, *M. leucogaster*, *M. bicolor*, and *M. fanjingshanensis* all are much larger (FA over 37 mm, Table 1); the similar-sized *M. shuipuensis* and *M. rongjiangensis* have an overall reddish dorsal fur, distally yellowish-gold ventral hairs, shorter ears, shorter FA, less convergent maxillary toothrow, and weaker P^4 (Table 1; Supplementary Figure S1 and Table S1).

Other species with a similarly developed P^4, which is basally much larger than C and P^2 (*M. aurata*, *M. harpioloides*, *M. chrysochaetes*, *M. eleryi*, *M. gracilis*, *M. recondita*) have a reddish dorsal pelage, weaker dentition, and domed braincase. With the exception of *M. recondita*, the above species also possess conspicuous shiny golden guard hairs on the dorsum in sharp contrast with the fur of *Murina jinchui* **sp. nov**.

The species *M. feae*, *M. beelzebub*, and *M. jaintiana* are characterized by similar, grayish dorsal and ventral fur, but all have a more domed braincase, and much less developed posterior upper premolars both in height and basal

dimensions.

Etymology: The species is named in honor of Professor Jinchu Hu, one of the founders of the Hetaoping Giant Panda Training Base and Wolong National Nature Reserve in China as well as a well-known giant panda expert, who has supported, encouraged, and actively participated in extensive ecological research in China, especially in Sichuan Province.

Natural history: Currently known only from the type locality, namely Hetaoping Giant Panda Training Base, Wolong National Nature Reserve, Wenchuan County, Sichuan Province, China. The *Murina jinchui* **sp**. **nov**. specimens were captured in harp traps set in moist evergreen and deciduous broadleaved forests (e.g., *Cyclobalanopsis*, *Quercus*, *Betula*) near the ruins of the original Giant Panda Breeding Center of the Hetaoping Giant Panda Training Base. Three *Rhinolophus ferrumequinum* and one *Pipistrellus* sp. were also caught at this site.

The existence of cryptic diversity within *Murina* is demonstrated by the large number of new species described from the Indomalayan region. China's wide variety of habitats, ranging from tropical to boreal forests and from grassland to desert, has greatly contributed to the richness of chiropteran resources. *Murina* species from China are recorded from temperate regions in the north to subtropical and tropical regions in the south and southwest (Jiang et al., 2015; Liu & Wu, 2019). This vast distribution, together with the many unexplored areas in regard to chiropterological surveys, implies an exceptionally high level of cryptic species diversity in tube-nose bats. Although molecular analysis using DNA barcoding, developed as a tool for rapid identification, can facilitate cryptic species recognition and improve understanding of biogeographical patterns (Csorba et al., 2011; Francis et al., 2010; Francis & Eger, 2012), taxonomic and systematic studies and species identification still depend on morphological data. For instance, species identification of *Murina* typically requires evaluation of morphological characters and availability of properly identified comparative material in museum collections, most of which is deposited in Europe and North America. Such predicaments may be abated in the future by reciprocation of 3D skull models of comparative material using high precision 3D scanners.

Mammalian fur/pelage within many species is subject to a considerable degree of intraspecific color variation (Corbet & Hill, 1992; Davis & Castleberry, 2010; Kries et al., 2018; Son et al., 2015); however, the color patterns of *Murina*, including overall dorsal and ventral aspects, banding of individual hairs, and presence and distribution of brightly colored guard hairs on forearm and/or hindfoot, appear to be stable within species. Therefore, coloration is a useable diagnostic tool for identifying *Murina* species in the field.

Although no sexual or intraspecific variations in pelage color were observed in the new species, sexual size dimorphism, a common phenomenon in *Murina* (Son et al., 2015), emerged during morphological analyses (Figure 1A–C, E; Table 1; Supplementary Figure S1). Females were significantly larger than males in measurements related to length and width of braincase, upper toothrow, and overall size of lower jaw (Table 1). This pattern of sexual dimorphism is suggested to have occurred under functional limitations and differed among skull regions (e.g., braincase and nasal chambers), therefore doesn't reflect simple allometric size changes.

SUPPLEMENTARY DATA

Supplementary data to this article can be found online.

COMPETING INTERESTS

The authors declare that they have no competing interests.

AUTHORS' CONTRIBUTIONS

W. H. Y., G. C., and Y. W. designed the study; W. H. Y. and Y. W. collected materials for the study; W. H. Y. and Y. W. performed morphometric and phylogenetic analyses; W.H.Y., G.C., and Y.W. interpreted the results and prepared the manuscript, photographs, and figures for the study. All authors read and approved the final version of the manuscript.

ACKNOWLEDGEMENTS

We are grateful to two anonymous referees for their constructive comments. We thank Prof. Yu-Chun Li from Shandong University, He-Ming Zhang and Ming-Chun Zhang from Wolong National Nature Reserve for their assistance during field work. We also thank Feng Li, Bo-Cheng Chen and Qiu-Ping Zhang for their help in field survey and assistance during lab work.

Wen-Hua Yu[1], Gabor Csorba[2], Yi Wu[1,*]

[1] *Key Laboratory of Conservation and Application in Biodiversity of South China*, *School of Life Sciences*, *Guangzhou University*, *Guangzhou* 510006, *China*

[2] *Department of Zoology*, *Hungarian Natural History Museum*, *Budapest H*-1088, *Hungary*

*Corresponding author, E-mail: wuyizhouq@263.net

REFERENCES

Chen J, Liu T, Deng HQ, Xiao N, Zhou J. 2017. A new species of *Murina* bats was discovered in Guizhou Province, China. *Cave Research*, **2**(1): 1−10.

Corbet GB, Hill JE. 1992. The Mammals of the Indomalayan Region. London: Natural History Museum.

Csorba G, Son NT, Saveng I, Furey NM. 2011. Revealing cryptic bat diversity: Three new *Murina* and redescription of *M. tubinaris* from Southeast Asia. *Journal of Mammalogy*, **92**(4): 891−904.

Csorba G, Thong VD, Bates PJJ, Furey NM. 2007. Description of a new species of *Murina* from Vietnam (Chiroptera: Vespertilionidae: Murininae). *Occasional Papers, Museum of Texas Tech University*, **268**: 1−9.

Davis AK, Castleberry SB. 2010. Pelage color of red bats *Lasiurus borealis* varies with body size: An image analysis of museum specimens. *Current Zoology*, **56**(4): 401−405.

Edgar RC. 2004. MUSCLE: multiple sequence alignment with high accuracy and high throughput. *Nucleic Acids Research*, **32**(5): 1792−1797.

Eger JL, Lim BK. 2011. Three new species of *Murina* from southern China (Chiroptera: Vespertilionidae). *Acta Chiropterologica*, **13**(2): 227−243.

Francis CM, Borisenko AV, Ivanova NV, Eger JL, Lim BK, Guillén-Servent

A, Kruskop SV, Mackie I, Hebert PD. 2010. The role of DNA barcodes in understanding and conservation of mammal diversity in southeast Asia. *PLoS One*, **5**: e12575−e12575.

Francis CM, Eger JL. 2012. A review of tube-nosed bats (*Murina*) from Laos with a description of two new species. *Acta Chiropterologica*, **14**(1): 15−38.

Furey NM, Thong VD, Bates PJJ, Csorba G. 2009. Description of a new species belonging to the *Murina* '*suilla*-group' (Chiroptera: Vespertilionidae: Murininae) from north Vietnam. *Acta Chiropterologica*, **11**(2): 225−236.

He F, Xiao N, Zhou J. 2015. A new species of *Murina* from China (Chiroptera: Vespertilionidae). *Cave Research*, **2**: 2−6.

Heaney LR, Balete DS, Alviola P, Rickart EA, Ruedi M. 2012. *Nyctalus plancyi* and *Falsistrellus petersi* (Chiroptera: Vespertilionidae) from Northern Luzon, Philippines: Ecology, phylogeny, and biogeographic implications. *Acta Chiropterologica*, **14**(2): 265−278.

Jiang ZG, Ma Y, Wu Y, Wang YX, Zhou KY, Liu SY, Feng Z. 2015. China's Mammal Diversity and Geographic Distribution. Beijing: Science Press. (in Chinese)

Jombart T. 2008. Adegenet: a R package for the multivariate analysis of genetic markers. *Bioinformatics*, **24**(11): 1403−1405.

Jombart T, Devillard S, Balloux F. 2010. Discriminant analysis of principal components: a new method for the analysis of genetically structured populations. *BMC Genetics*, **11**: 94.

Kries K, Barros MAS, Duytschaever G, Orkin JD, Janiak MC, Pessoa DMA, Melin AD. 2018. Colour vision variation in leaf-nosed bats (Phyllostomidae): Links to cave roosting and dietary specialization. *Molecular Ecology*, **27**(18): 3627−3640.

Kruskop SV, Eger JL. 2008. A new species of tube-nosed bat *Murina* (Vespertilionidae, Chiroptera) from Vietnam. *Acta Chiropterologica*, **10**(2): 213−220.

Kuo HC, Fang YP, Csorba G, Lee LL. 2009. Three new species of *Murina* (Chiroptera: Vespertilionidae) from Taiwan. *Journal of Mammalogy*, **90**(4): 980−991.

Kuo HC, Soisook P, Ho YY, Csorba G, Wang CN, Rossiter SJ. 2017. A taxonomic revision of the *Kerivoula hardwickii* complex (Chiroptera: Vespertilionidae) with the description of a new species. *Acta Chiropterologica*, **19**(1): 19−39.

Lack JB, Bussche RAVD. 2010. Identifying the confounding factors in resolving phylogenetic relationships in Vespertilionidae. *Journal of Mammalogy*, **91**(6): 1435−1448.

Lanfear R, Calcott B, Ho SYW, Guindon S. 2012. Partitionfinder: combined selection of partitioning schemes and substitution models for phylogenetic analyses. *Molecular Biology and Evolution*, **29**(6): 1695−1701.

Lanfear R, Frandsen PB, Wright AM, Senfeld T, Calcott B. 2017. PartitionFinder 2: New methods for selecting partitioned models of evolution for molecular and morphological phylogenetic analyses. *Molecular Biology and Evolution*, **34**(3): 772−773.

Liu SY, Wu Y. 2019. Handbook of the Mammals of China. *Fuzhou: Straits Press*: 520.

Maeda K, Matsumura S. 1998. Two new species of Vespertilionid bats, *Myotis* and *Murina* (Vespertilionidae: Chiroptera) from Yanbaru, Okinawa Island, Okinawa Prefecture, Japan. *Zoological Science*, **15**(2): 301−307.

Roehrs ZP, Lack JB, Van Den Bussche RA. 2010. Tribal phylogenetic relationships within Vespertilioninae (Chiroptera: Vespertilionidae) based on mitochondrial and nuclear sequence data. *Journal of Mammalogy*, **91**(5): 1073−1092.

Ruedi M, Biswas J, Csorba G. 2012. Bats from the wet: two new species of Tube-nosed bats (Chiroptera: Vespertilionidae) from Meghalaya, India. *Revue Suisse de Zoologie*, **119**(1): 111−135.

Simmons NB. 2005. Order Chiroptera. *In*: Wilson DE, Reeder DM. Mammal Species of the World: a Taxonomic and Geographic Reference, 3rd edn. Baltimore: The Johns Hopkins University Press, 2142.

Soisook P, Karapan S, Satasook C, Bates PJ. 2013a. A new species of *Murina* (Mammalia: Chiroptera: Vespertilionidae) from peninsular Thailand. *Zootaxa*, **3746**(4): 567−579.

Soisook P, Karapan S, Satasook C, Thong VD, Khan FAA, Maryanto I, Csorba G, Furey N, Aul B, Bates PJJ. 2013b. A review of the *Murina cyclotis* complex (Chiroptera: Vespertilionidae) with descriptions of a new species and subspecies. *Acta Chiropterologica*, **15**(2): 271−292.

Son NT, Csorba G, Tu VT, Thong VD, Wu Y, Harada M, Oshida T, Endo H, Motokawa M. 2015. A new species of the genus *Murina* (Chiroptera: Vespertilionidae) from the central highlands of Vietnam with a review of the subfamily Murininae in Vietnam. *Acta Chiropterologica*, **17**(2): 201−232.

Stamatakis A, Hoover P, Rougemont J. 2008. A rapid bootstrap algorithm for the RAxML web servers. *Systematic Biology*, **57**(5): 758−771.

Zeng X, Chen J, Deng HQ, Xiao N, Zhou J. 2018. A new species of *Murina* from China (Chiroptera: Vespertilionidae). *Ekoloji*, **103**(27): 9−16.